Oxidation of butane-2,3-dione at high pressure: Implications for ketene chemistry

Xiaoyuan Zhang, Maxence Lailliau, Yuyang Li, Yumeng Zhu, Zehua Feng, Wei Li, Philippe Dagaut

Oxidation of butane-2,3-dione at high pressure: Implications for ketene chemistry

Xiaoyuan Zhang [a], Maxence Lailliau [b], Yuyang Li [c,*], Yumeng Zhu [a], Zehua Feng [a], Philippe Dagaut [b,*]

[a] *Department of Thermal Science and Energy Engineering, University of Science and Technology of China, Hefei 230026, P. R. China*

[b] *C.N.R.S., Institut de Combustion, Aérothermique, Réactivité et Environnement, 1C, Avenue de la Recherche Scientifique, 45071 Orléans Cedex 2, France*

[c] *Institute of Aerospace Propulsion, School of Mechanical Engineering, Shanghai Jiao Tong University, Shanghai 200240, P. R. China*

Abstract: Ketene (CH_2CO) mechanism is a building block for developing combustion kinetic models of practical fuels. To revisit the combustion chemistry related to ketene, oxidation experiments of butane-2,3-dione (diacetyl, $CH_3COCOCH_3$), considered as an effective precursor of CH_2CO, are conducted in a jet-stirred reactor (JSR) at 10 bar and temperatures ranging from 650 to 1160 K. Identification and quantification of intermediates are achieved by Fourier transform infrared spectrometry, gas chromatography, and mass spectrometry. A kinetic model of diacetyl is constructed based on recent theoretical and modeling studies on diacetyl and ketene, which has been validated against the present data and experimental data of diacetyl and CH_2CO in literature. Generally, the present model can adequately predict most of them, and better predict the methyl-related intermediates under wide pyrolysis and combustion conditions than previous models. Based on modeling analyses, the unimolecular decomposition reaction of diacetyl is the dominant reaction pathway for fuel consumption under different equivalence ratio conditions, especially at high temperatures. Under lean conditions, both the H-atom abstraction reactions by methyl (i.e. $CH_3COCOCH_3 + CH_3 = CH_4 +$

* Corresponding authors. E-mails: yuygli@sjtu.edu.cn (YL), dagaut@cnrs-orleans.fr (PD).

CH_2CO + CH_3CO, R3) and by OH (i.e. $CH_3COCOCH_3$ + OH = H_2O + CH_2CO + CH_3CO, R5) are important for diacetyl consumption, while under rich conditions R5 becomes negligible. As the most important intermediates in diacetyl oxidation, the main consumption pathways of CH_2CO and CH_3 are dependent on the equivalence ratio conditions. Under lean conditions, CH_2CO mainly reacts with OH to produce CH_2OH and CO (i.e. CH_2CO + OH = CH_2OH + CO, R10), while methyl reacts with HO_2 to produce CH_3O and OH (i.e. CH_3 + HO_2 = CH_3O + OH, R20). In contrast, under rich conditions, the addition-elimination reaction between CH_2CO and H becomes competitive with R10, while the CH_3 self-combination producing C_2H_6 plays a more important role than the CH_3 oxidation pathway R20. Sensitivity analysis of CH_2CO shows that not only the reactions of CH_2CO, but also those of CH_3 are sensitive to CH_2CO formation. This is because CH_3 related reactions influence the distribution of radical pool, which determines the oxidation reactivity of the reaction system.

Keywords: Diacetyl; ketene; jet-stirred reactor oxidation; high pressure; kinetic model

Novelty and Significance Statement

Ketene (CH_2CO) is an important intermediate in the combustion of practical fuels. An accurate CH_2CO mechanism is a building block for their model development. However, direct experiments for CH_2CO are difficult due to its high reactivity, limiting the development of CH_2CO mechanism for a long time. Butane-2,3-dione (diacetyl, $CH_3COCOCH_3$) is considered as an effective CH_2CO precursor. This work reports the first investigation on diacetyl oxidation at high pressure, extending previous experimental conditions to 10 bar. A kinetic model of diacetyl is developed with particular concerns on CH_2CO chemistry, and comprehensively validated against both the present and previous experimental data. Sensitivity analysis shows that the experimental data measured in this work are helpful to constrain the uncertainties of CH_2CO mechanism. Insight into the reaction kinetics of CH_2CO at high pressure and different equivalence ratio conditions is also derived from the present

model.

Author Contributions

Xiaoyuan Zhang: Conceptualization, Investigation, Validation, Writing-original draft. **Maxence Lailliau:** Investigation, Data curation. **Yuyang Li:** Conceptualization, Writing-reviewing and editing, Funding acquisition. **Yumeng Zhu:** Investigation. **Zehua Feng:** Investigation. **Philippe Dagaut:** Conceptualization, Methodology, Writing-reviewing and editing.

1. Introduction

Butane-2,3-dione (diacetyl, $CH_3COCOCH_3$) has received particular attention from the combustion community in recent years [1-6], since it can serve as an effective precursor of methyl radical (CH_3) and ketene (CH_2CO). Both CH_3 and CH_2CO mechanisms are the building blocks for developing the combustion kinetic models of fundamental fuels [7]. In addition, they are key intermediates in the pyrolysis and combustion of large hydrocarbon [8] and oxygenated fuels [9], and their related reactions play an important role in determining the critical combustion parameters [10, 11].

Our previous work focused on the CH_3-related growth chemistry by studying the pyrolysis of diacetyl at pressures ranging from 0.04 to 10 bar [2]. The pressure dependency of the carbon chain growth from CH_3 was discussed based on both experimental measurements and modeling analyses. Unlike the unimolecular decomposition kinetics of diacetyl (R1-R2), which mainly produces CH_3, the H-atom abstraction kinetics of diacetyl (R3-R5) can stimulate the formation of CH_2CO. As a continuation of our previous work, the present work focuses on CH_2CO chemistry by investigating the oxidation of diacetyl, which creates reaction conditions that favor H-atom abstraction kinetics. Previous studies on the diacetyl oxidation are mainly under flame conditions. Christensen and Konnov [4] measured the laminar flame speeds of diacetyl/air at atmospheric pressure using heat flux method,

which provided indirect experimental data for the validation of CH_2CO mechanism. Sun et al. [3] and Lin et al. [1] measured the speciation data in laminar premixed diacetyl flames at both low and atmospheric pressure, respectively, to refine the CH_2CO mechanism. Besides these indirect measurements, Hidaka et al. [12] also directly measured the speciation data in the shock tube oxidation of CH_2CO at temperatures ranging from 1050 to 2050 K and pressures ranging from 1 to 3 bar. The above measurements can provide valuable validation targets for CH_2CO chemistry at high temperature and low to atmospheric pressures. However, neither the direct nor indirect experimental studies on CH_2CO oxidation at intermediate temperatures and high pressures are available in literature, hindering the development of CH_2CO mechanism under practical ignition conditions.

$$CH_3COCOCH_3\ (+M) = 2CH_3CO\ (+M) \quad \text{(R1)}$$

$$CH_3CO\ (+M) = CH_3 + CO\ (+M) \quad \text{(R2)}$$

$$CH_3COCOCH_3 + CH_3 = CH_4 + CH_2CO + CH_3CO \quad \text{(R3)}$$

$$CH_3COCOCH_3 + H = H_2 + CH_2CO + CH_3CO \quad \text{(R4)}$$

$$CH_3COCOCH_3 + OH = H_2O + CH_2CO + CH_3CO \quad \text{(R5)}$$

In addition, for the model development on diacetyl and ketene, previous models are only validated against specific experimental targets under limited combustion conditions. Konnov and coworkers developed the diacetyl model based on rate constant evaluation [4] and theoretical calculations [6]. Besides the validation targets of CH_2CO, only the laminar flame speeds of diacetyl and other carbonyl fuels were incorporated for model validation. Sun et al. [3] and Lin et al. [1] also developed the diacetyl model based on theoretical calculations and uncertainty analyses. However, only the flame speciation data and the laminar flame speed data were selected for model validation. Minwegen et al. [13] developed CH_2CO pyrolysis model by applying ab initio quantum chemistry calculations and focused solely on the validation against CH_2CO pyrolysis conditions. Comprehensive kinetic models, validated

against experimental targets under wide pyrolysis and oxidation conditions, have not been established yet.

In this work, the oxidation experiments of diacetyl are conducted in a jet-stirred reactor (JSR) at 10 bar and temperatures ranging from 650 to 1160 K, extending previous experimental conditions to intermediate temperatures and high pressures. Fourier transform infrared spectroscopy (FTIR), gas chromatography (GC), and mass spectrometry (MS) are introduced for the identification and quantification of both primary and secondary products. Based on recent theoretical calculation and modeling studies on both diacetyl [3, 5] and CH_2CO [6, 14, 15], a kinetic model is developed to investigate the conversion of diacetyl, as well as the formation and consumption of CH_2CO. The model is validated against the present data and experimental data of diacetyl and CH_2CO in literature. The kinetics on the decomposition of diacetyl and the oxidation of CH_2CO at high pressure are discussed with a special emphasis on the effects of equivalence ratio.

2. Experimental method

The JSR experiments were carried out at C.N.R.S. in Orléans, France. The detailed descriptions on the experimental apparatus can be found in our previous work [16]. Briefly, the reactor consists of a fused silica sphere with a volume of ~38 cm^3. It is settled inside a stainless-steel jacket to resist high pressure. Liquid diacetyl (purity 97%, provided by Sigma-Aldrich) and auxiliary N_2 are introduced into the reactor through a heated vaporizer. The Fuel-N_2 mixture flows through a fused silica capillary (1 mm I.D.) until it is mixed with the primary N_2 and O_2 just before entering the reactor. Stirring is achieved by four nozzles with 1 mm orifice inside the reactor sphere. The pressure inside the reactor is kept at 10 bar. The initial mole fraction of diacetyl is 1000 ppm and the total flow rates of the reacting mixture are adjusted at each temperature to keep a constant residence time of 700 ms. The conditions of the present experiment, along with those of our previous pyrolysis experiments [2] are summarized

in Table 1.

The reacting mixtures are sampled using a low-pressure sonic probe. The detection of CO, CO_2, H_2O, and formaldehyde (CH_2O) is performed with online FTIR, while other hydrocarbons and oxygenated products are quantified with GCs. Two GCs equipped with flame ionization detectors (FID) are used in this work. One is equipped with a DB624 column to quantify oxygenated compounds (such as CH_2CO, CH_3CHO, CH_3COCH_3, and $CH_3COCOCH_3$), while the other one is equipped with a CP-Al_2O_3/KCl column to quantify hydrocarbons (such as CH_4, C_2H_4, C_2H_6, and C_3H_8). Identification of the products is achieved by GC combined with quadrupole MS. The uncertainties are within ±15% for most of the oxidation products except for CH_2CO, which is estimated to be a factor of 2 because of lack of direct calibration and the use of the carbon equivalent method [17]. The mole fractions of the measured species can be found in the *Supplemental Materials*.

Table 1. Experimental conditions in present JSR oxidation experiment and previous pyrolysis experiment [2].

Fuel (ppm)	O_2 (%)	N_2 (%)	T (K)	P (bar)	ϕ	τ (ms)	References
1000	0.9	99	710–1100	10	0.5	700	This work
1000	0.225	99.675	650–1160	10	2.0	700	This work
2000	0	99.8	650-1130	10	∞	700	[2]

3. Kinetic modeling

3.1. Base mechanism

The present model is developed based on our previous diacetyl pyrolysis model [2], which was constructed from models of methanol [18], methane (CH_4) [19], and CH_3CHO [20]. The methanol model [18] was developed with special concerns on CO/CH_2O/CH_3OH chemistry, while the methane (CH_4) [19] and CH_3CHO [20] models revisited the CH_3 chemistry under flame and ignition conditions, respectively. In our previous diacetyl pyrolysis study [2], the CH_3 related growth mechanism was examined, including the sub-mechanisms of ethane (C_2H_6), ethylene (C_2H_4), acetylene (C_2H_2), propane (C_3H_8), propene (C_3H_6), propyne (PC_3H_4), allene (AC_3H_4), 1,3-butadiene (C_4H_6), and

vinylacetylene (C_4H_4), as well as the sub-mechanism of benzene formation. Comprehensive model validation for the base mechanism can be found in [2, 18-20].

3.2. Sub-mechanism of diacetyl

In our previous pyrolysis model, the rate constant of the unimolecular decomposition reaction of diacetyl (R1) is adopted from Yang et al. [5], which is retained in the present model. Recently, Sun et al. [3] investigated the bimolecular reactions between diacetyl and radicals (i.e. H and CH_3) theoretically. The rate constants of both H-atom abstraction reactions (R3 and R4) and the addition-elimination reactions (R6 and R7) are calculated, which seems to be more reliable than the evaluation and optimization results [4, 5]. In this work, we adopt the theoretical calculation results for R4, R6, and R7 from Sun et al. [3], while retain the rate constant of R3 based on the optimization results of Yang et al. [5], since the computed rate constant by Sun et al. [3] is abnormally fast. Their computed H-atom abstraction reaction of diacetyl by CH_3 (i.e. R3), is only 4 times and 20% slower than that by H atom (i.e. R4) at 1000 and 2000 K, respectively. While the rate constant differences of the H-atom abstraction reactions by H and CH_3 are generally more than one order of magnitude based on reaction rate rules established by pioneer modeling studies [21-24]. Therefore, we adopted another rate constant source from Yang et al. [5], which is 5-6 times lower than that computed by Sun et al. and obeys the rate rules constructed by pioneer modeling studies [21-24]. Details will be discussed in the following sections. Under oxidation conditions, the reactions between diacetyl and OH are also important. The rate constant of H-atom abstraction reaction by OH (R5) is retained in the present model, which is taken from Christensen and Konnov [4], while that of the addition-elimination reaction (R8) is taken from estimated results by Sun et al. [3] to better predict the formation of acetic acid (CH_3COOH) in laminar premixed flame experiments [1, 3].

$$CH_3COCOCH_3 + CH_3 = CH_3COCH_3 + CH_3CO \quad \text{(R6)}$$

$CH_3COCOCH_3 + H = CH_3CHO + CH_3CO$ (R7)

$CH_3COCOCH_3 + OH = CH_3COOH + CH_3CO$ (R8)

3.3. Sub-mechanism of CH_2CO

CH_2CO is one of the most important intermediates in diacetyl pyrolysis. In our previous model, the sub-mechanism of CH_2CO was mainly referred to the modeling work of Christensen and Konnov [25, 26]. Recently, Minwegen et al. [13] developed a ketene pyrolysis model by applying ab initio quantum chemistry calculations. Most of important CH_2CO pyrolysis reactions are computed in their study, which are adopted in this work to update the submechanism of ketene pyrolysis [25, 26]. Surprisingly, in the pyrolysis model from Minwegen et al. [13], the H addition-elimination reaction of CH_2CO (R9) is missing. Since this reaction converts reactive H atom to less reactive CH_3 radical and has lower energy barrier than that of H-atom abstraction reaction, we retain this reaction in the present model using the theoretical calculation results from [27]. Similar to R9, CH_3 radical can convert CH_2CO to CO and C_2H_5. This reaction is also incorporated and its rate constant is taken from the theoretical calculation study of Zaleski et al. [28]. Under oxidation conditions, the reactions between CH_2CO and OH (R10-R13) are also responsible for chain propagation. However, large discrepancies exist in their rate constants among the available literature [6, 29-31]. More recent study from Savchenkova et al. [6] implemented higher level of theory and their computed results can better predict the laminar flame speeds of diacetyl/air, and thus their temperature- and pressure-dependent rate constants for $CH_2OH + OH$ are adopted in the present model.

$CH_2CO + H = CH_3 + CO$ (R9)

$CH_2CO + OH = CH_2OH + CO$ (R10)

$CH_2CO + OH = HCCO + H_2O$ (R11)

$CH_2CO + OH = CH_3 + CO_2$ (R12)

$CH_2CO + OH = CH_2COOH$ (R13)

HO_2 plays an important role under intermediate-temperature and high-pressure conditions. Therefore, the reactions between CH_2CO and HO_2 are also important under the present conditions. Bai et al. [15] recently computed the reaction pathways of $CH_2CO + HO_2$ and obtained the temperature- and pressure-dependent rate constants. Among them, R14-R16 have large branching ratios at atmospheric pressure and temperatures above 600 K. In the present model, these reaction channels and their rate constants are considered based on their theoretical calculations.

$CH_2CO + HO_2 = CH_3CO + O_2$ (R14)

$CH_2CO + HO_2 = CH_2O + CO + OH$ (R15)

$CH_2CO + HO_2 = oxiranone + OH$ (R16)

Ethynyloxy radical (HCCO) is produced from the H-atom abstraction reactions of CH_2CO, which is also an important radical in acetylene oxidation. Besides CH_2O, the reactions of HCCO with reactive radicals and oxygen offer additional pathways for CO formation. Despite of their important role in combustion chemistry, the measured rate constants for HCCO reactions are scarce. According to the calculation work from Minwegen et al. [13], HCCO can proceed self-combination reaction to produce 1,4-dioxo-1,3-butadiene, which then decomposes to cyclopropenone. This reaction sequence is not included in this work, since under the present investigated conditions, R9 dominates the CH_2CO+H reaction while HCCO formation channel from the H-atom abstraction reaction has a minor contribution, i.e. less than 10%. Therefore, the self-combination reaction of HCCO radical probably has very limited contribution. In the present model, recently calculated rate constants at high level of theory are adopted for HCCO + H [32], HCCO + O_2 [33], HCCO + OH [34], and HCCO + HO_2 [14]. HCO can be an intermediate produced via these HCCO-related reactions (i.e. HCCO+O_2 = O+CO+HCO). Since HCO is a weakly bound free radical, the prompt dissociation reaction pathways

of HCO (i.e. HCCO+O_2 = O+CO+H+CO) are incorporated, and the rate constants are taken from the theoretical calculation study of Labbe et al. [35]. The files for the reaction mechanism, thermodynamic data, and transport data are provided in the *Supplementary Materials*.

3.4. Simulation methods

For the JSR simulation, the Perfectly Stirred Reactor module in the CHEMKIN-PRO software [36] is used. Fixing gas temperature is selected as the problem type, while the transient solver is adopted. The residence time is used as an input parameter for the JSR simulation instead of setting volume and inlet flow rate. For the simulations of the flow reactor pyrolysis experiments, Plug Flow Reactor module is adopted with the measured centerline temperature profiles as input parameters. Shock tube simulations are performed using a Batch Reactor module with the problem type of constrain volume and solve energy equation. Premixed laminar burner-stabilized flame module is used to simulate the flame speciation experiments. The measured temperature profiles are incorporated to account for the heat loss. Laminar flame speed calculation is based on solving the energy equation. Soret effects and mixed-averaged transport are considered. Grid-independence is achieved using the GRAD and CURV to be 0.05. Detailed simulation methods can be found in our previous work [37].

4. Results and discussion

4.1. Comparison between measured and predicted results

The measured and predicted mole fraction profiles of major species, i.e. diacetyl, CO, H_2O, CO_2, CH_4, and CH_2CO, are presented in Fig. 1. Besides the present model, predicted results by recent 2022 Lin model [1] and 2020 Konnov model [6] are also plotted for comparison. All the three models can well predict the conversion of diacetyl, which are very close under both lean and rich conditions. The predicted discrepancies become larger for the products (CO, H_2O, and CO_2) above 1000 K. The present model can slightly better predict the consumption of CO and the formation of CO_2 under lean

conditions. Unlike the fuel, the products formation under different equivalence ratio conditions presents obvious differences, which can be captured by all the three models. For the two intermediates CH_4 and CH_2CO, the present model can reasonably predict their formation, while the Konnov model [6] generally overpredict it. More recent Lin model [1] can reasonably predict the formation of CH_2CO while predicts a faster formation rate of CH_4 under rich condition.

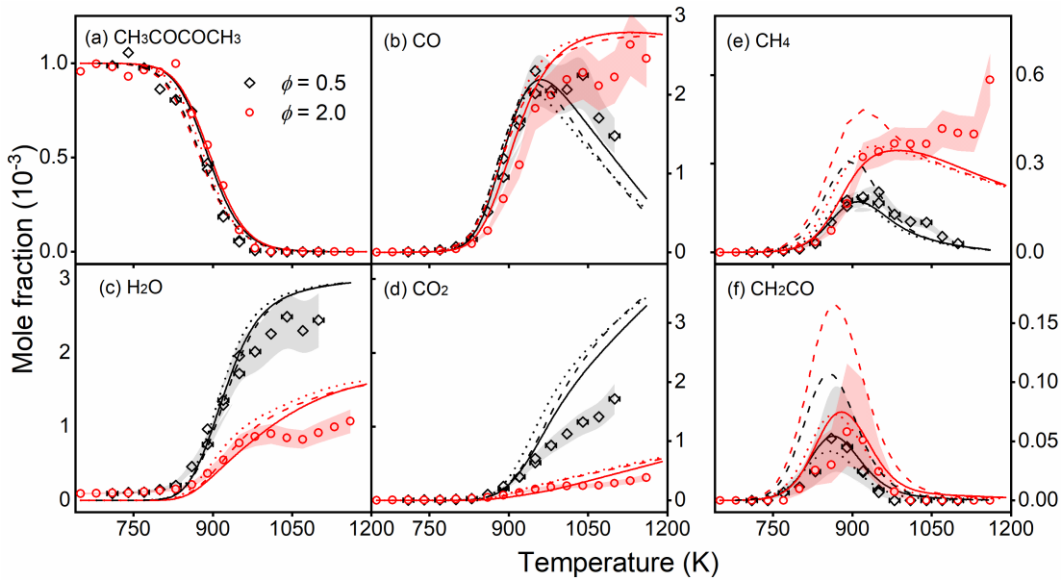

Figure 1 Measured (symbols) and predicted (lines) mole fraction profiles of (a) diacetyl, (b) CO, (c) H_2O, (d) CO_2, (e) CH_4, and (f) CH_2CO in the JSR oxidation of diacetyl at 10 bar. The experimental uncertainties are shown with shadows. Solid, dotted, and dashed lines represent the predicted results by the present model, 2022 Lin model [1], and 2020 Konnov model [6], respectively.

Minor oxygenated intermediates including acetaldehyde (CH_3CHO), acetone (CH_3COCH_3), and CH_2O are also measured in this work under both lean and rich conditions. The performance of the present model and previous models [1, 6] is shown in Fig. 2. Generally, all the models underpredict the yields of these products. Compared with previous models, the present model greatly improves the prediction of CH_3COCH_3, as seen from Fig. 2(b). Besides, all the models predict larger yields of

CH_3CHO and CH_3COCH_3 under rich conditions than lean conditions, which is consistent with the measured results. In contrast, for the formation of CH_2O, the present experimental data show that its peak mole fraction under lean conditions is larger than that under rich condition, while all the three models predict an opposite trend, as shown in Fig. 2(c). Figure 3 presents the measured and predicted results for minor hydrocarbon intermediates. Under lean conditions, only C_2 hydrocarbons are measured, while under rich conditions both C_2 and C_3 hydrocarbons are measured. The present model is capable to predict all these hydrocarbon intermediates except ethylene (C_2H_4). In contrast, previous models [1, 6] underpredict all of them.

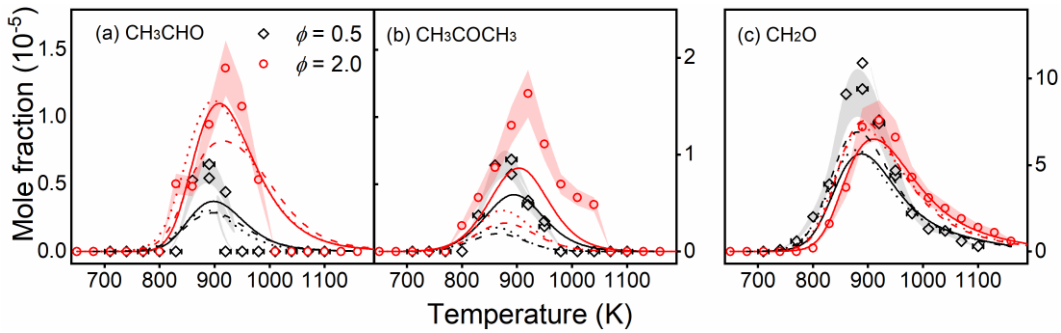

Figure 2 Measured (symbols) and predicted (lines) mole fraction profiles of (a) CH_3CHO, (b) CH_3COCH_3, and (c) CH_2O in the JSR oxidation of diacetyl at 10 bar. The experimental uncertainties are shown with shadows. Solid, dotted, and dashed lines represent the predicted results by the present model, 2022 Lin model [1], and 2020 Konnov model [6], respectively.

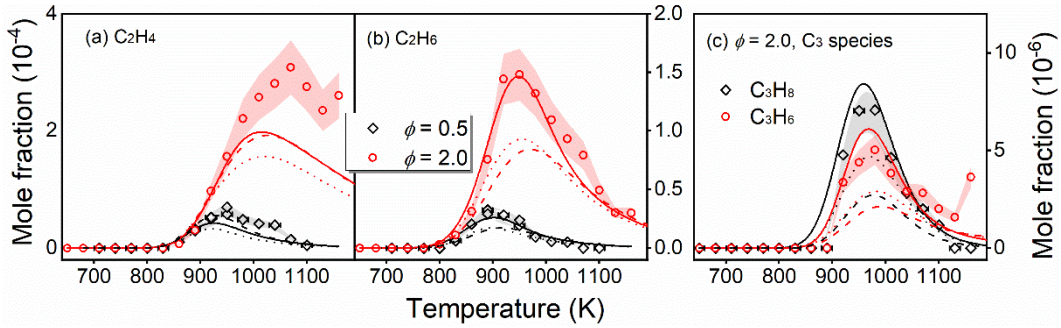

Figure 3 Measured (symbols) and predicted (lines) mole fraction profiles of (a) C_2H_4, (b) C_2H_6, and (c) C_3H_6 and C_3H_8 in the JSR oxidation of diacetyl at 10 bar. The experimental

uncertainties are shown with shadows. Solid, dotted, and dashed lines represent the predicted results by the present model, 2022 Lin model [1], and 2020 Konnov model [6], respectively.

In summary, for most of the products, all the three models can predict their trends under different equivalence ratio conditions. Compared with previous models [1, 6], the present model can better capture the yields of CH_3COCH_3, and hydrocarbon products. The reasons for the model improvements will be discussed in next section based on the rate of production (ROP) and sensitivity analyses.

4.2. Conversion of diacetyl

According to the ROP analysis, the carbon flux of diacetyl under 10 bar and 920 K is presented in Fig. 4. H-atom abstraction reactions and unimolecular decomposition reactions are the major pathways to consume diacetyl, while the addition-elimination reactions play a minor role. All the three pathways lead to the formation of CH_3CO, which quickly decomposes to produce CH_3 and CO. Therefore, CH_3 is the most important intermediate in diacetyl oxidation, which is also an important precursor of C_2 species and CH_2O. In addition, the other important intermediate, CH_2CO, can be produced via the H-atom abstraction reactions of diacetyl by various radicals. The oxidation kinetics of CH_2CO and CH_3 can be found in the next section. The total contribution of the H-atom abstraction reactions of diacetyl (including R3-R5) are similar under the present lean and rich conditions, as well as the unimolecular decomposition reaction R1. This can explain the weak equivalence ratio effects of diacetyl conversion observed in the present experiment, as seen from Fig. 1(a).

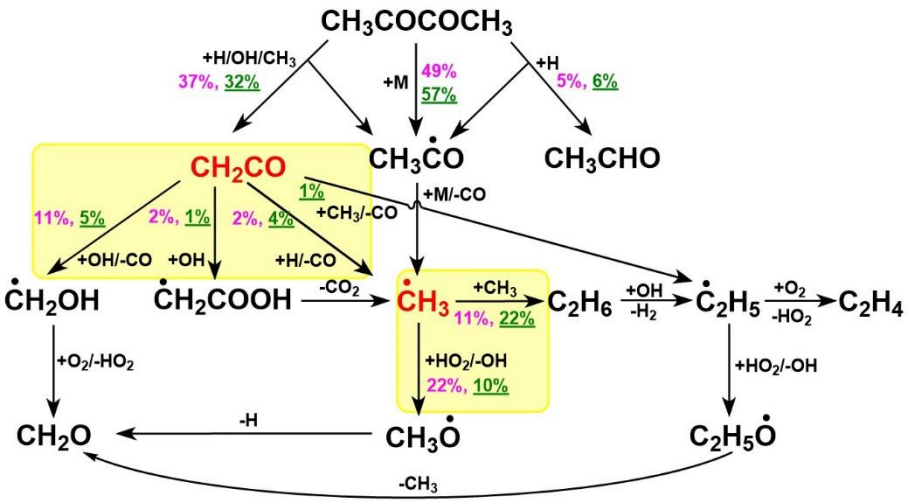

Figure 4 Carbon flux of diacetyl based on ROP analysis of the present model at 10 bar and 920 K. Numbers with and without underline represent the equivalence ratios of 2.0 and 0.5, respectively.

However, when considering the specific reactions that consume diacetyl, the effects of equivalence ratio become obvious. Figure 5 presents the ROP and sensitivity analysis results of diacetyl under lean, rich, and pyrolysis conditions. Under all the equivalence ratio conditions, diacetyl is mainly consumed via R1 and R3. At $\phi = 0.5$, R1 is more important than R3 over the whole diacetyl conversion ratio, while with the equivalence ratio becomes richer, R3 becomes more competitive. R5 is the H-atom abstraction reaction of diacetyl by OH, which is only important under lean condition. The sensitivity analysis results are consistent with those of ROP. R5 is only sensitive under lean condition.

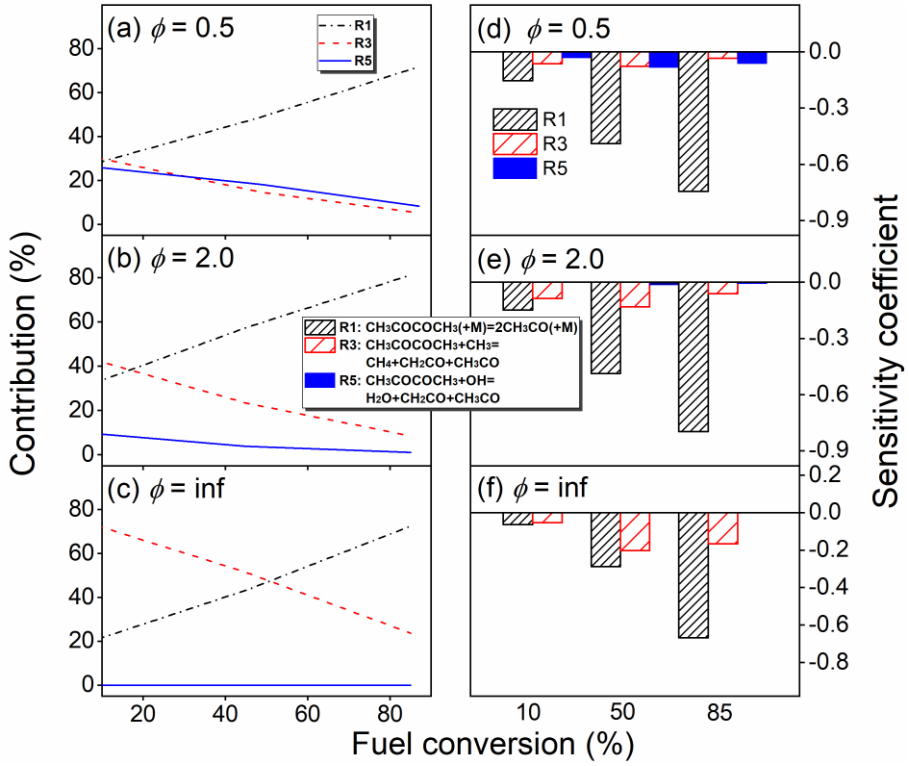

Figure 5 Left: ROP analysis of diacetyl versus the fuel conversion ratio at (a) ϕ = 0.5, (b) ϕ = 2.0, and (c) pyrolysis condition; Right: Sensitivity analysis of diacetyl at fuel conversion ratios of 10%, 50%, and 85% under (d) lean (ϕ = 0.5), (e) rich (ϕ = 2.0), and (f) pyrolysis condition.

Based on the above analysis, R3 plays a critical role in accurately predicting the fuel consumption under various conditions. It is also an important pathway for CH_3 consumption and CH_4 formation. In addition, R3 competes with the addition-elimination reaction R6 ($CH_3COCOCH_3 + CH_3 = CH_3COCH_3 + CH_3CO$), R17, and R18. Therefore, R3 is critical to predict the mole fractions of CH_4, CH_3COCH_3, C_2H_6, and C_3H_8 measured in this work. Sun et al. [3] computed the rate constant of R3 based on quantum chemistry at high level of theory. Their results were adopted by 2020 Konnov model [6] and 2022 Lin model [1]. Yang et al. [5] optimized the rate constant of R3 based on their shock tube pyrolysis experiments, which is taken in the present model. The rate constant of R3 obtained from the two sources [3, 5] has large discrepancy. The computed result from Sun et al. [3] is 5-6 times higher than that from Yang et al. [5] at temperatures ranging from 500 to 2200 K. The 2020 Konnov model

[6] and 2022 Lin model [1] both overpredict the formation of CH_4 while underpredict the formation of CH_3COCH_3, C_2H_6, and C_3H_8, indicating that the computed rate constant of R3 by Sun et al. [3] is too high. Therefore, we adopted the optimized result from Yang et al. [5] in the present model, which greatly improves the prediction of CH_4, CH_3COCH_3, and other C_2 and C_3 products simultaneously.

$$CH_3 + CH_3 (+M) = C_2H_6 (+M) \quad \text{(R17)}$$

$$CH_3 + C_2H_5 (+M) = C_3H_8 (+M) \quad \text{(R18)}$$

4.3. Consumption of critical intermediates

4.3.1. CH_2CO consumption

Under the present conditions, CH_2CO is mainly consumed through three pathways, including two addition-elimination reactions R9 ($CH_2CO + H = CH_3 + CO$) and R10 ($CH_2CO + OH = CH_2OH + CO$) and one addition reaction R13 ($CH_2CO + OH = CH_2COOH$). Under lean conditions, addition-elimination reaction between CH_2CO and OH (R10) is dominant, while the other two reactions R9 and R13 play a minor role. In contrast, under rich condition, the addition-elimination reaction between CH_2CO and H (R9) becomes competitive with R10, which are the two main pathways to consume CH_2CO. Addition reaction R13 and addition-elimination reaction ($CH_2CO + CH_3 = C_2H_5 + CO$)play a minor role. Therefore, the consumption pathways of CH_2CO are dependent on the equivalence ratio. At $\phi = 0.5$, hydroxymethyl (CH_2OH) is the dominant product from CH_2CO. CH_2OH proceeds an H-atom abstraction reaction by O_2 to produce CH_2O and HO_2 through R19. Under the present intermediate-temperature and high-pressure conditions, HO_2 is a critical chain carrier that can be easily converted to OH via the reaction sequence $HO_2 \rightarrow H_2O_2 \rightarrow OH$. HO_2 is more produced under lean conditions, leading to faster formation rates of intermediates than rich conditions, which is consistent with the measured results.

$$CH_2OH + O_2 = CH_2O + HO_2 \quad \text{(R19)}$$

4.3.2. CH_3 consumption

CH_3 is mainly produced from both fuel via R1 and CH_2CO via R9. Similar to CH_2CO, the consumption pathways of CH_3 are also dependent on equivalence ratio conditions, as seen from Fig. 4. There are two main consumption pathways of CH_3, that is, the oxidation pathway through C_1 intermediates and the self-combination pathway through C_2 intermediates. It can be observed that the oxidation pathway and self-combination pathway are more important under lean and rich conditions, respectively. Therefore, more carbon flux is converted to C_2 intermediates under rich conditions, which is consistent with the measured results, as seen from Fig. 3(a, b). As mentioned above, HO_2 is a critical radical under the present conditions, which can be converted to two OH radicals mediated by H_2O_2. Besides this chain-branching pathway, HO_2 can also be converted to OH through R20 and R21, which are important oxidation pathways of CH_3 and C_2H_5, respectively. The decomposition of CH_3O and C_2H_5O both leads to the formation of CH_2O.

$$CH_3 + HO_2 = CH_3O + OH \quad \text{(R20)}$$

$$C_2H_5 + HO_2 = C_2H_5O + OH \quad \text{(R21)}$$

4.3.3. Sensitivity analysis results

Based on the present model, the sensitivity analyses of CH_2CO under different temperature and equivalence ratio conditions are performed. As seen from Fig. 6, both CH_2CO and CH_3 related reactions present large sensitivity coefficients. At 860 K, R10 ($CH_2CO + OH = CH_2OH + CO$) presents the largest negative sensitivity under both lean and rich conditions, while at 980 K and ϕ = 2.0, R9 ($CH_2CO + H = CH_3 + CO$) also presents large negative sensitivity, indicating that the experimental data under these conditions can be helpful to constrain the uncertainties of CH_2CO mechanism. In addition, CH_3 related reactions are also sensitive to CH_2CO formation, since its conversion greatly influences the distribution of radical pool. The reaction producing OH (R20) promotes the reactivity

of the oxidation system and contributes to CH_2CO consumption via R10, and thus it has negative sensitivity coefficient for CH_2CO. In contrast, chain-termination reaction (R22) inhibits OH formation, and thus have positive sensitivity coefficients for CH_2CO.

$$CH_3 + HO_2 = CH_4 + O_2 \qquad \text{(R22)}$$

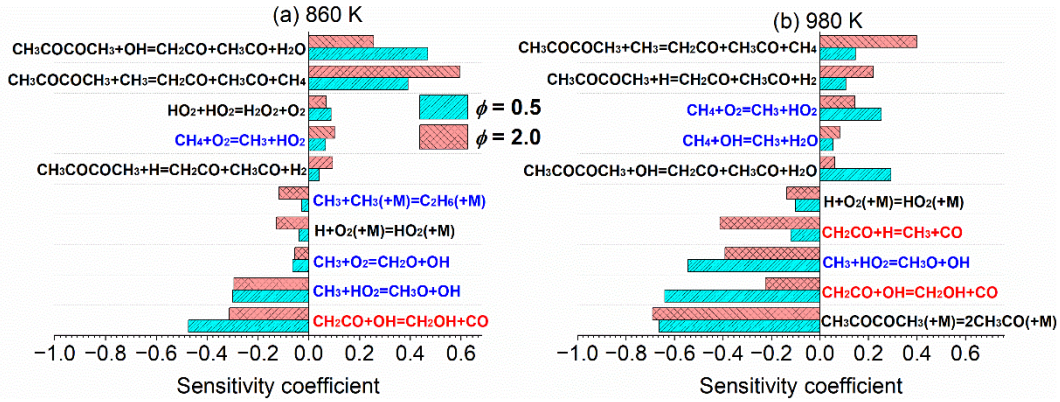

Figure 6 Sensitivity analysis of CH_2CO based on the present model at (a) 860 K and (b) 980 K. Dense and sparse bars represent equivalence ratios at ϕ = 0.5 and ϕ = 2.0, respectively. CH_2CO and CH_3 related reactions are highlighted with red and blue colors, respectively.

4.4. Additional validations

4.4.1. Validations against diacetyl experimental targets

Besides the present experimental data, the present model is also validated against the experimental data of diacetyl in literature, including pyrolysis speciation data in both flow reactor and JSR, flame speciation data at both low and atmospheric pressure, and laminar flame speeds at various unburned temperatures, as listed in Table 2. In our previous pyrolysis study on diacetyl, the speciation data were measured in a flow reactor at low to atmospheric pressures and a JSR at 10 bar. Mole fraction profiles of oxygenated intermediates such as CH_2CO, CH_3CHO, and CH_3COCH_3, as well as C_1-C_6 hydrocarbon products, are used to further validate the present model. As seen from Figs. 7-9, compared with previous models [1, 6], the present model can better predict the formation of CH_4, CH_2CO, C_2H_6, and C_3H_8. As mentioned above, these products are directly or indirectly related to R3 ($CH_3COCOCH_3$

+ CH_3 = CH_4 + CH_2CO + CH_3CO). The 2022 Lin model [1] and 2020 Konnov model [6] adopted a much higher rate constant for R3, which leads to the overprediction of CH_4 and CH_2CO. Since R3 consumes CH_3, which is competitive with R17 (CH_3 + CH_3 (+M) = C_2H_6 (+M)) and R18 (CH_3 + C_2H_5 (+M) = C_3H_8 (+M)), the reaction pathways of methyl growth are inhibited, leading to the underprediction of C_2H_6 and C_3H_8.

Table 2. Validation targets of diacetyl and ketene for the present model

Fuel	Method	Mixture	T (K)	P (bar)	ϕ	References
diacetyl	Flow reactor	$(CH_3CO)_2$/Ar	780-1520	0.04-1	∞	[2]
	JSR	$(CH_3CO)_2/N_2$	650-1130	10	∞	[2]
	JSR	$(CH_3CO)_2/O_2/N_2$	650-1160	10	0.5-2	This work
	Burner-stabilized flame	$(CH_3CO)_2/O_2$/Ar	493-2432	0.02	1.2	[3]
	Burner-stabilized flame	$(CH_3CO)_2/O_2$/Ar	368-2087	1	0.5-1.9	[1]
	Laminar flame speed	$(CH_3CO)_2$/air	298-338	1	0.7-1.5	[4]
ketene	Shock tube	CH_2CO/Ar	1725	7	∞	[38]
	Shock tube	CH_2CO/Ar	1670	2	∞	[39]
	Shock tube	CH_2CO/Ar	1250-1550	4	∞	[40]
	Shock tube	CH_2CO/Ar	1200-1500	2	∞	[41]
	Shock tube	CH_2CO/O_2/Ar	1050-2050	1.1-3	1-4	[12]

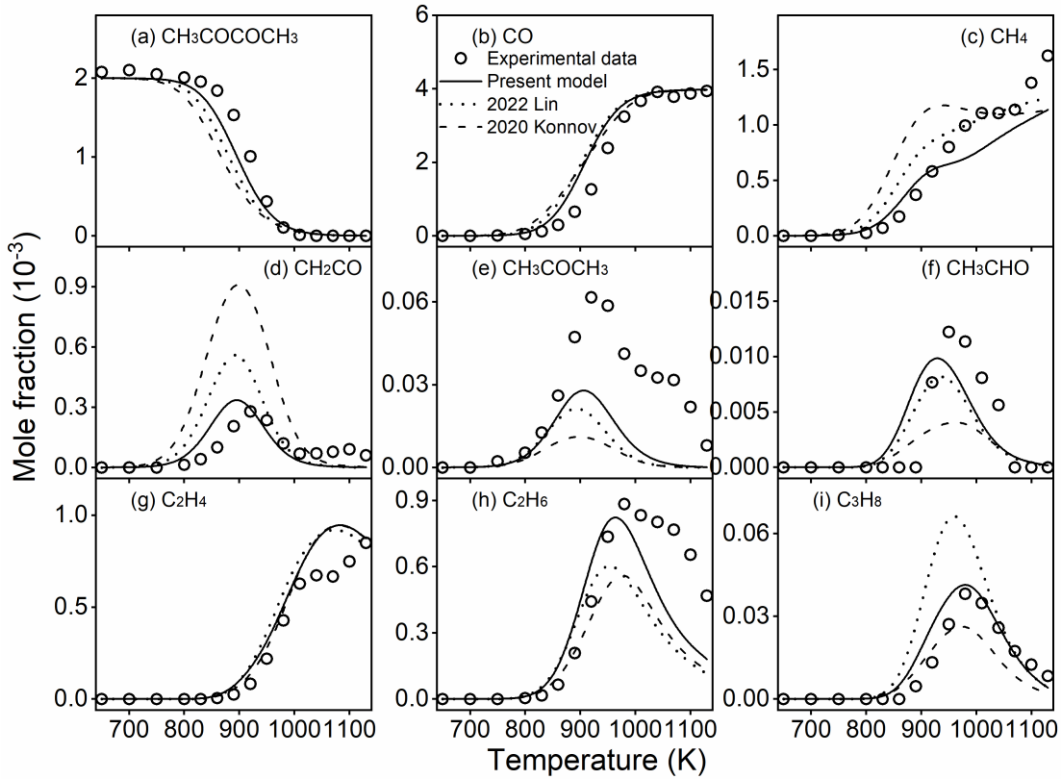

Figure 7 Measured (symbols) [2] and predicted (lines) mole fraction profiles of (a) $CH_3COCOCH_3$,

(b) CO, (c) CH_4, (d) CH_2CO, (e) CH_3COCH_3, (f) CH_3CHO, (g) C_2H_4, (h) C_2H_6, and (i) C_3H_8 in the pyrolysis of diacetyl in a JSR at 10 bar. Solid, dotted, and dashed lines represent the predicted results by the present model, 2022 Lin model [1], and 2020 Konnov model [6], respectively.

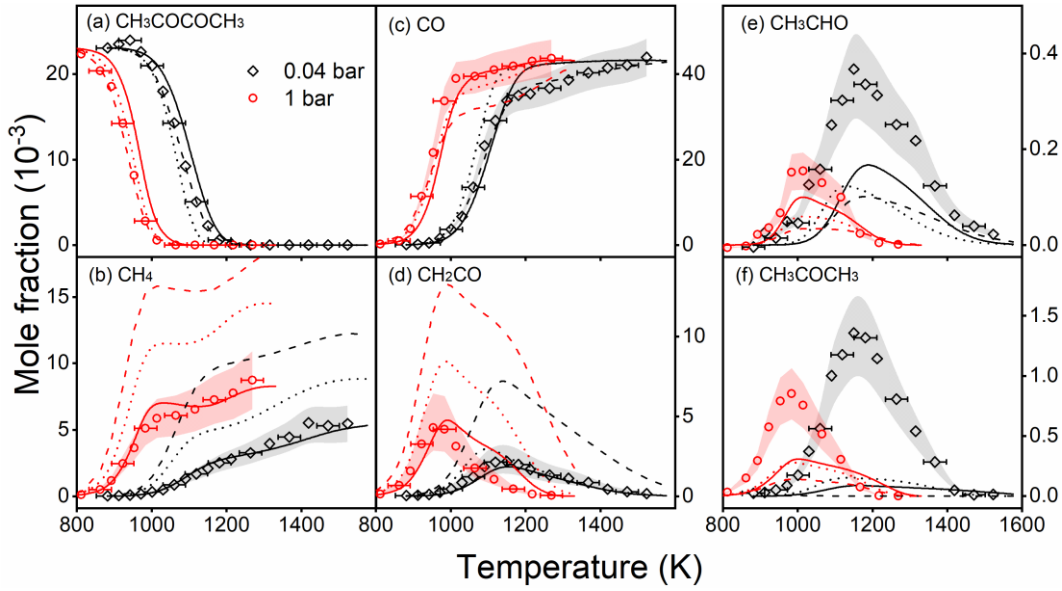

Figure 8 Measured (symbols) [2] and predicted (lines) mole fraction profiles of (a) $CH_3COCOCH_3$, (b) CH_4, (c) CO, (d) CH_2CO, (e) CH_3CHO, and (f) CH_3COCH_3 in the pyrolysis of diacetyl in a flow reactor at 0.04 and 1 bar. Solid, dotted, and dashed lines represent the predicted results by the present model, 2022 Lin model [1], and 2020 Konnov model [6], respectively.

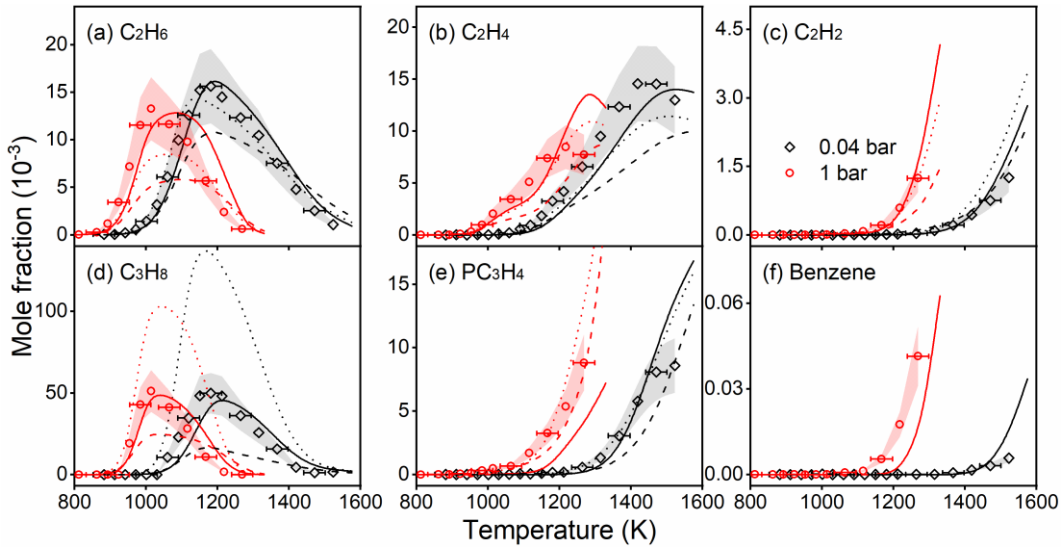

Figure 9 Measured (symbols) [2] and predicted (lines) mole fraction profiles of (a) C_2H_6, (b) C_2H_4,

(c) C_2H_2, (d) C_3H_8, (e) propyne (PC_3H_4), and (f) benzene in the pyrolysis of diacetyl in a flow reactor at 0.04 and 1 bar. Solid, dotted, and dashed lines represent the predicted results by the present model, 2022 Lin model [1], and 2020 Konnov model [6], respectively.

Besides pyrolysis experimental targets, the present model is also validated against the speciation data measured in burner-stabilized premixed flames [1, 3] and laminar flame speed data measured with heat flux method [4]. In the flame speciation experiments, besides the products measured in this work, CH_3 and CH_3COOH are measured in literature [1, 3]. Compared with 2022 Lin model [1] and 2020 Konnov model [6], the present model can better predict the formation of CH_3 and CH_3COOH respectively under both lean and rich conditions, as seen from Figs. 10 and S1-S3 in the *Supplementary Materials*. The comparison between the measured and predicted laminar flame speeds of diacetyl/air are presented in Fig. 11 and Figs. S4-S5 in the *Supplementary Materials*. It shows that the present model can capture the position of peak laminar flame speed and reasonably predict the laminar flame speeds under both lean and rich conditions, improving the predictions under rich conditions compared to previous model.

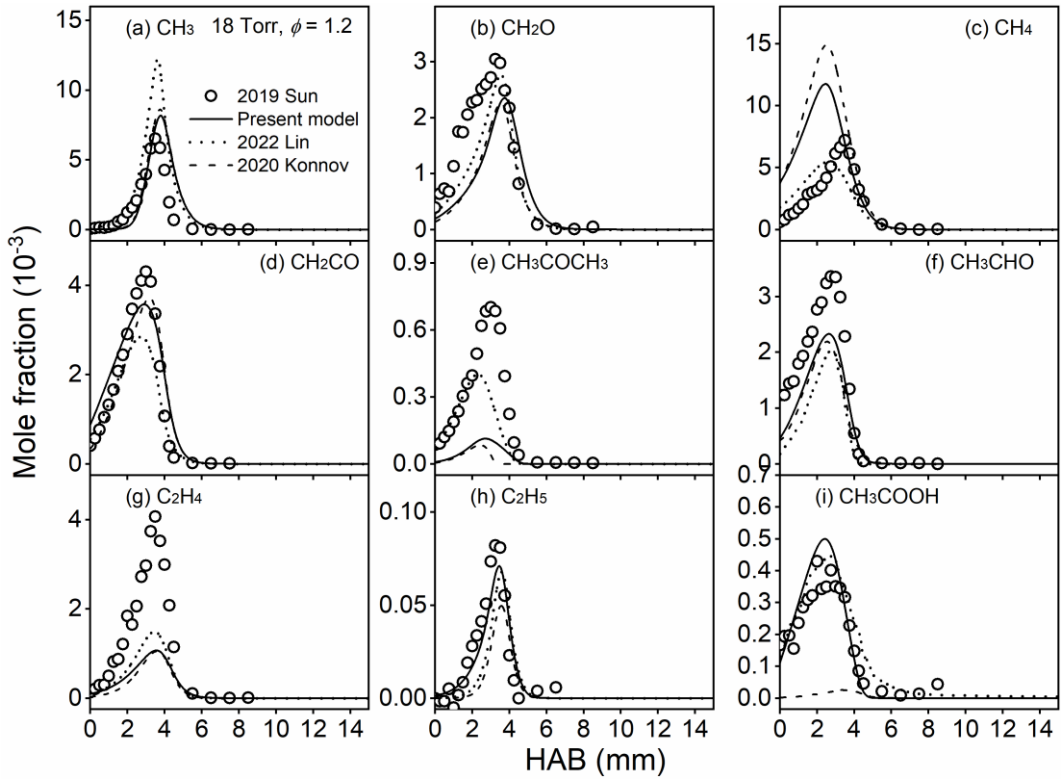

Figure 10 The measured (symbols) [3] and predicted (lines) mole fraction profiles in a burner-stabilized premixed flame at 18 Torr and ϕ = 1.2. Solid, dotted and dashed lines represent the predicted results by the present, 2022 Lin model [1] and 2020 Konnov model [6], respectively.

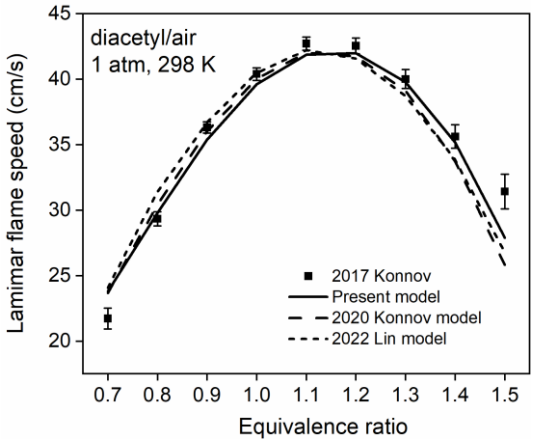

Figure 11 The measured (symbols) [4] and predicted (lines) laminar flame speeds of diacetyl/air at unburned temperature of 298 K and unburned pressure of 1 bar. Solid, dotted, and dashed lines represent the predicted results by the present model, 2022 Lin model [1], and 2020 Konnov model [6], respectively.

4.4.2. Validations against ketene experimental targets

Besides the experimental targets of diacetyl, as one of the most important intermediates in diacetyl oxidation, the experimental targets of ketene are also selected to validate the present model, as listed in Table 2, including both pyrolysis and oxidation experimental data. Besides the 2020 Konnov model [6] and 2022 Lin model [1], the recent ketene pyrolysis model developed by Minwegen et al. [13] is also selected for comparison. The comparison between the measured and predicted results are presented in Figs. 12-13 and Figs. S6-S8 in the *Supplementary Materials*. Generally, the present model can reasonably predict the consumption of CH_2CO and formation of the major products, i.e. CH_4, CO, and CO_2. However, for the prediction of minor hydrocarbon intermediates, e.g. C_2H_6, the present

model, as well as previous models [1, 6, 13], fail to accurately capture their formation. It is noticed that although the present model mainly adopted the submechanism of ketene pyrolysis from Minwegen et al. [13], the present model has better predictions on CO_2, H and CO compared with Minwegen model [13]. This is mainly result from the incorporation of R9 ($CH_2CO+H = CO+CH_3$) and the different base mechanism in this model. Since the measured speciation data for ketene are very limited, more experiments on ketene pyrolysis and oxidation are highly required to further constrain the uncertainties of CH_2CO mechanism.

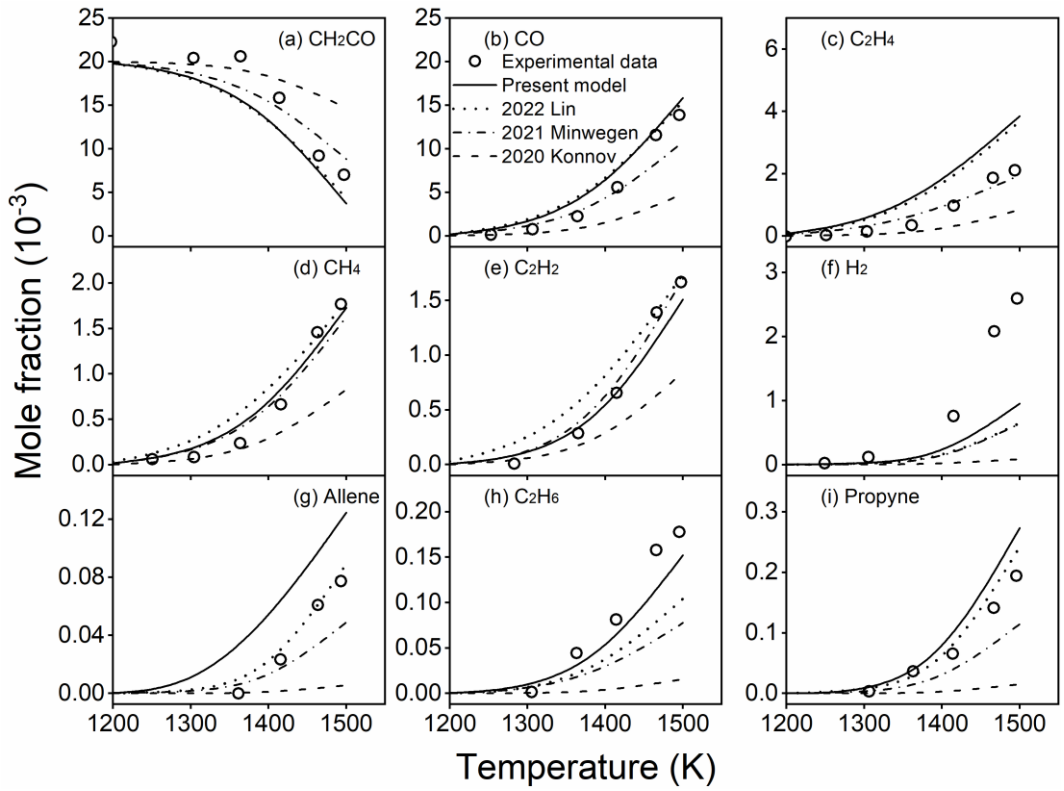

Figure 12 Comparison between measured [41] (symbols) and predicted (lines) mole fraction profiles in shock tube pyrolysis of CH_2CO at 2 atm. The mixture is 2.2% CH_2CO/98% Ar. The effective heating times are 1.97 ms (1200 K), 1.89 ms (1300 K), 1.8 ms (1400 K), and 1.71 ms (1500 K). Solid, dotted, dash dot, and dashed lines represent the predicted results by the present model, 2022 Lin model [1], 2021 Minwegen model [13], and 2020 Konnov model [6], respectively.

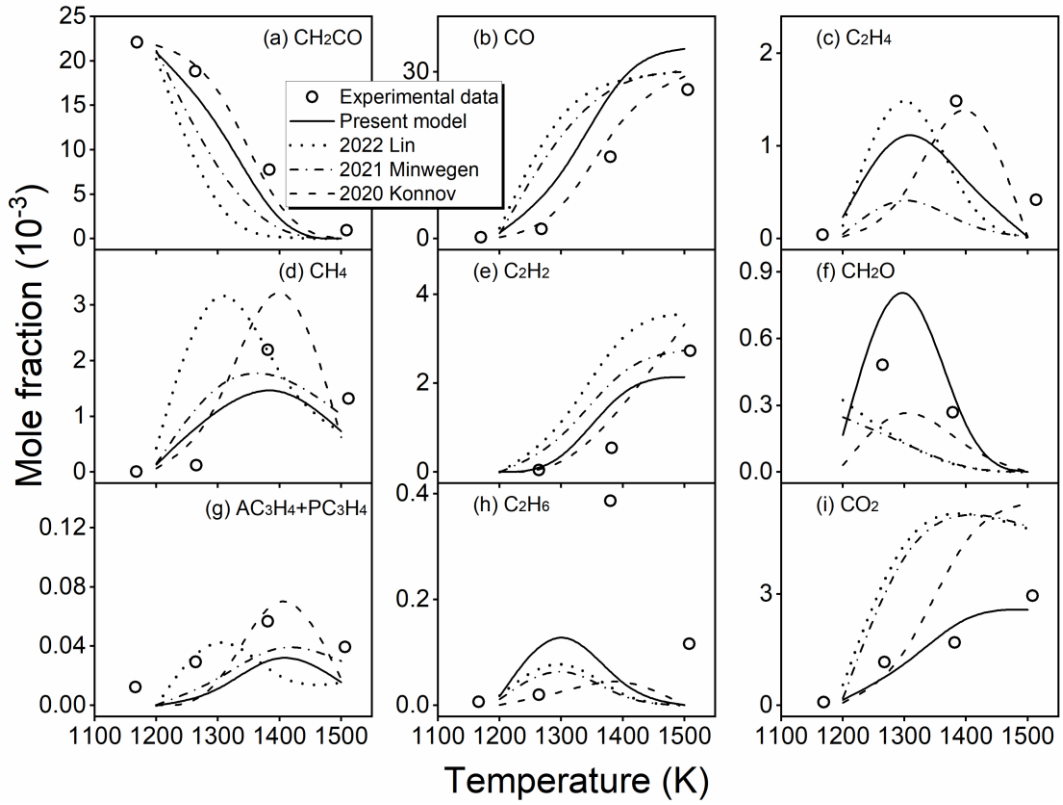

Figure 13 Comparison between measured [12] (symbols) and predicted (lines) mole fraction profiles in shock tube oxidation of CH_2CO at 2 atm. The mixture is 2.2% CH_2CO/1.2% O_2/98% Ar. The effective heating times are 1.97 ms (1200 K), 1.89 ms (1300 K), 1.8 ms (1400 K), and 1.71 ms (1500 K). Solid, dotted, dash dot, and dashed lines represent the predicted results by the present model, 2022 Lin model [1], 2021 Minwegen model [13], and 2020 Konnov model [6], respectively.

5. Conclusions

The oxidation of diacetyl was investigated in a JSR at 10 bar and temperatures ranging from 650 to 1160 K. Intermediates were measured using several diagnostic methods, including FTIR, GC, and GC/MS. A kinetic model of diacetyl was constructed based on recent theoretical and modeling studies on diacetyl and ketene. The model was validated against the present data and experimental data of diacetyl and CH_2CO in literature. Generally, the present model can adequately predict most of them, and better predict the methyl-related intermediates, such as C_2H_6, C_3H_6, C_3H_8 etc., under wide

pyrolysis and combustion conditions compared with previous models.

Based on the present model, the unimolecular decomposition reaction of diacetyl (R1) is the dominant reaction pathway for fuel consumption under different equivalence ratio conditions, especially at high temperature, which leads to the formation of CH_3. The total contributions of the H-atom abstraction reactions of diacetyl (R3-R5) are similar under lean and rich conditions. Under lean conditions, both R3 and R5 are important for diacetyl consumption, while under rich conditions R3 is the only important H-atom abstraction reaction. These H-atom abstraction reactions are responsible for the formation of both CH_2CO and CH_3.

The main consumption pathways of CH_2CO and CH_3 are dependent on the equivalence ratio conditions. Under lean conditions, CH_2CO mainly reacts with OH to produce CH_2OH and CO, while CH_3 mainly reacts with HO_2 to produce CH_3O and OH. In contrast, under rich conditions, the addition-elimination reaction between CH_2CO and H becomes competitive to consume CH_2CO, while CH_3 self-combination reaction producing C_2H_6 is the dominant CH_3 consumption pathway. Sensitivity analysis of CH_2CO shows that not only the reactions of CH_2CO, but also those of CH_3 are sensitive to CH_2CO consumption. This is because the reactions of CH_3 influence the distribution of radical pool, especially the OH formation, which consumes CH_2CO via the addition-elimination reaction R10.

Acknowledgements

The authors are grateful for the funding support from National Natural Science Foundation of China (52206164), Science Center for Gas Turbine Project (P2022-B-II-017-001), and Oceanic Interdisciplinary Program of Shanghai Jiao Tong University (SL2022ZD104). Xiaoyuan Zhang appreciates the China Scholarship Council (CSC) for support. Maxence Lailliau appreciates the Region Centre for a Ph.D. grant and the Labex Caprysses (ANR-11-LABX-0006-01) for support.

References

[1] K. Lin, A.M. Dmitriev, W. Sun, A.G. Shmakov, D.A. Knyazkov, B. Yang, Improving the predictive accuracy for ketene

in diacetyl laminar premixed flames: Experiment and model analysis, J. Phys. Chem. A 126 (2022) 9475-9484.
[2] X. Zhang, M. Lailliau, C. Cao, Y. Li, P. Dagaut, W. Li, T. Li, J. Yang, F. Qi, Pyrolysis of butane-2,3-dione from low to high pressures: Implications for methyl-related growth chemistry, Combust. Flame 200 (2019) 69-81.
[3] W. Sun, J. Wang, C. Huang, N. Hansen, B. Yang, Providing effective constraints for developing ketene combustion mechanisms: A detailed kinetic investigation of diacetyl flames, Combust. Flame 205 (2019) 11-21.
[4] M. Christensen, A.A. Konnov, Laminar burning velocity of diacetyl + air flames. Further assessment of combustion chemistry of ketene, Combust. Flame 178 (2017) 97-110.
[5] X. Yang, A.W. Jasper, J.H. Kiefer, R.S. Tranter, The dissociation of diacetyl: A shock tube and theoretical study, J. Phys. Chem. A 113 (2009) 8318-8326.
[6] A.S. Savchenkova, A.S. Semenikhin, I.V. Chechet, S.G. Matveev, A.M. Mebel, A.A. Konnov, Revisiting diacetyl and acetic acid flames: The role of the ketene + OH reaction, Combust. Flame 218 (2020) 28-41.
[7] W.K. Metcalfe, S.M. Burke, S.S. Ahmed, H.J. Curran, A hierarchical and comparative kinetic modeling study of C1 − C2 hydrocarbon and oxygenated fuels, Int. J. Chem. Kinet. 45 (2013) 638-675.
[8] X. Zhang, S.M. Sarathy, A lumped kinetic model for high-temperature pyrolysis and combustion of 50 surrogate fuel components and their mixtures, Fuel 286 (2021) 119361.
[9] X. Zhang, S.M. Sarathy, High-temperature pyrolysis and combustion of C_5-C_{19} fatty aid methyl esters (FAMEs): A lumped kinetic modeling study, Energy Fuels 35 (2021) 19553-19567.
[10] W.K. Metcalfe, W.J. Pitz, H.J. Curran, J.M. Simmie, C.K. Westbrook, The development of a detailed chemical kinetic mechanism for diisobutylene and comparison to shock tube ignition times, Proc. Combust. Inst. 31 (2007) 377-384.
[11] E. Ranzi, A. Frassoldati, R. Grana, A. Cuoci, T. Faravelli, A.P. Kelley, C.K. Law, Hierarchical and comparative kinetic modeling of laminar flame speeds of hydrocarbon and oxygenated fuels, Prog. Energ. Combust. Sci. 38 (2012) 468-501.
[12] Y. Hidaka, K. Kimura, K. Hattori, T. Okuno, Shock tube and modeling study of ketene oxidation, Combust. Flame 106 (1996) 155-167.
[13] H. Minwegen, M. Döntgen, Y. Fenard, P. Morsch, K.A. Heufer, Proceeding on the riddles of ketene pyrolysis by applying ab initio quantum chemical computational methods in a detailed kinetic modeling study, Proc. Combust. Inst. 38 (2021) 749-755.
[14] J. Guo, N. Tan, L. Chen, S. Tang, A. Tang, Reactions of ethynyloxy radical with hydroperoxyl radical: Bridging theoretical reaction dynamics and chemical modeling of combustion, ChemPhysChem 25 (2024) e202300515.
[15] J. Bai, C.-W. Zhou, L. Yang, Theoretical study on the reaction of ketene + HO_2: From electronic structure to model applications, Combust. Flame 232 (2021) 111502.
[16] P. Dagaut, M. Cathonnet, J.P. Rouan, R. Foulatier, A. Quilgars, J.C. Boettner, F. Gaillard, H. James, A jet-stirred reactor for kinetic studies of homogeneous gas-phase reactions at pressures up to ten atmospheres (≈1 MPa), J. Phys. E: Sci. Instrum. 19 (1986) 207-209.
[17] J. Bugler, A. Rodriguez, O. Herbinet, F. Battin-Leclerc, C. Togbé, G. Dayma, P. Dagaut, H.J. Curran, An experimental and modelling study of n-pentane oxidation in two jet-stirred reactors: The importance of pressure-dependent kinetics and new reaction pathways, Proc. Combust. Inst. 36 (2017) 441-448.
[18] X. Zhang, G. Wang, J. Zou, Y. Li, W. Li, T. Li, H. Jin, Z. Zhou, Y.-Y. Lee, Investigation on the oxidation chemistry of methanol in laminar premixed flames, Combust. Flame 180 (2017) 20-31.
[19] X. Zhang, B. Mei, S. Ma, H. Pan, H. Wang, Y. Li, Experimental and kinetic modeling investigation on laminar flame propagation of CH_4/CO mixtures at various pressures: Insight into the transition from CH_4-related chemistry to CO-related chemistry, Combust. Flame 209 (2019) 481-492.
[20] X. Zhang, L. Ye, Y. Li, Y. Zhang, C. Cao, J. Yang, Z. Zhou, Z. Huang, F. Qi, Acetaldehyde oxidation at low and intermediate temperatures: An experimental and kinetic modeling investigation, Combust. Flame 191 (2018) 431-441.
[21] E. Ranzi, C. Cavallotti, A. Cuoci, A. Frassoldati, M. Pelucchi, T. Faravelli, New reaction classes in the kinetic modeling of low temperature oxidation of n-alkanes, Combust. Flame 162 (2015) 1679-1691.
[22] S.M. Sarathy, P. Oßwald, N. Hansen, K. Kohse-Höinghaus, Alcohol combustion chemistry, Prog. Energy Combust. Sci. 44 (2014) 40-102.

[23] L. Cai, H. Pitsch, Mechanism optimization based on reaction rate rules, Combust. Flame 161 (2014) 405-415.
[24] C.K. Westbrook, W.J. Pitz, O. Herbinet, H.J. Curran, E.J. Silke, A comprehensive detailed chemical kinetic reaction mechanism for combustion of n-alkane hydrocarbons from n-octane to n-hexadecane, Combust. Flame 156 (2009) 181-199.
[25] M. Christensen, A.A. Konnov, Laminar burning velocity of diacetyl+air flames. Further assessment of combustion chemistry of ketene, Combust. Flame 178 (2017) 97-110.
[26] M. Christensen, A.A. Konnov, Laminar burning velocity of acetic acid + air flames, Combust. Flame 170 (2016) 12-29.
[27] J.P. Senosiain, S.J. Klippenstein, J.A. Miller, Pathways and rate coefficients for the decomposition of vinoxy and acetyl radicals, J. Phys. Chem. A 110 (2006) 5772-5781.
[28] D.P. Zaleski, R. Sivaramakrishnan, H.R. Weller, N.A. Seifert, D.H. Bross, B. Ruscic, K.B. Moore, III, S.N. Elliott, A.V. Copan, L.B. Harding, S.J. Klippenstein, R.W. Field, K. Prozument, Substitution reactions in the pyrolysis of acetone revealed through a modeling, experiment, theory paradigm, J. Am. Chem. Soc. 143 (2021) 3124-3142.
[29] B. Xu, J. Garrec, A. Nicolle, M. Matrat, L. Catoire, Temperature and pressure dependent rate coefficients for the reaction of ketene with hydroxyl radical, J. Phys. Chem. A 123 (2019) 2483-2496.
[30] C. Cavallotti, M. Pelucchi, A. Frassoldati, Analysis of acetic acid gas phase reactivity: Rate constant estimation and kinetic simulations, Proc. Combust. Inst. 37 (2019) 539-546.
[31] C. Oehlers, F. Temps, H.G. Wagner, M. Wolf, Kinetics of the reaction of OH radicals with CH_2CO, Bunsenges. Phys. Chem. 96 (1992) 171-175.
[32] P.-C. Nam, P. Raghunath, L.K. Huynh, S. Xu, M.C. Lin, Ab initio chemical kinetics for the HCCO + H reaction, Combust. Sci. Technol. 188 (2016) 1095-1114.
[33] S.J. Klippenstein, J.A. Miller, L.B. Harding, Resolving the mystery of prompt CO_2: The HCCO+O_2 reaction, Proc. Combust. Inst. 29 (2002) 1209-1217.
[34] S.-Z. Xiong, Q. Yao, Z.-R. Li, X.-Y. Li, Reaction of ketenyl radical with hydroxyl radical over $C_2H_2O_2$ potential energy surface: A theoretical study, Combust. Flame 161 (2014) 885-897.
[35] N.J. Labbe, R. Sivaramakrishnan, C.F. Goldsmith, Y. Georgievskii, J.A. Miller, S.J. Klippenstein, Weakly bound free radicals in combustion: “Prompt” dissociation of formyl radicals and its effect on laminar flame speeds, J. Phys. Chem. Lett. 7 (2016) 85-89.
[36] CHEMKIN-PRO 15092, Reaction Design: San Diego, 2009.
[37] X. Zhang, S.P. Moosakutty, R.P. Rajan, M. Younes, S.M. Sarathy, Combustion chemistry of ammonia/hydrogen mixtures: Jet-stirred reactor measurements and comprehensive kinetic modeling, Combust. Flame 234 (2021) 111653.
[38] H. Wagner, F. Zabel, Zum thermischen zerfall von keten in der gasphase, Ber. Bunsenges. Phys. Chem. 75 (1971) 114-118.
[39] P. Frank, K.A. Bhaskaran, T. Just, High-temperature reactions of triplet methylene and ketene with radicals, J. Phys. Chem. 90 (1986) 2226-2231.
[40] M. Tsuda, K. Kuratani, Thermal decomposition of ketene in shock waves, Bull. Chem. Soc. Jpn. 41 (1968) 53-60.
[41] Y. Hidaka, K. Kimura, H. Kawano, High-temperature pyrolysis of ketene in shock waves, Combust. Flame 99 (1994) 18-28.